J. Phys. B: At. Mol. Opt. Phys. **32** (1999) 2139–2152. Printed in the UK PII: S0953-4075(99)98886-7

Electron-impact excitation of Mg-like ions

D C Griffin†, N R Badnell‡, M S Pindzola§ and J A Shaw§

† Department of Physics, Rollins College, Winter Park, FL 32789, USA
‡ Department of Physics and Applied Physics, University of Strathclyde, Glasgow G4 0NG, UK
§ Department of Physics, Auburn University, Auburn, AL 36849, USA

Received 3 November 1998, in final form 8 January 1999

Abstract. In a recent paper (1998 *J. Phys. B: At. Mol. Opt. Phys.* **31** 3713–27), we described an intermediate-coupling frame transformation (ICFT) method based on multi-channel quantum defect theory that allows one to generate accurate level-to-level excitation data from unphysical K-matrices calculated in pure LS-coupling. In this paper, we consider ICFT R-matrix close-coupling calculations of effective collision strengths for the Mg-like ions Si^{2+}, Ar^{6+}, Ti^{10+} and Fe^{14+}. In order to further demonstrate the level of accuracy of this method, we compare our ICFT effective collision strengths with those determined from a full Breit–Pauli R-matrix calculation for Fe^{14+}. We also consider the use of our radiative rates and effective collision strengths in conjunction with a collisional–radiative program to generate line-emission intensity ratios as a function of density and temperature. The full set of energies, radiative rates, and effective collision strengths for these four ions have been made available on the Internet.

1. Introduction

The Breit–Pauli R-matrix method (see, for example, Berrington *et al* 1995) provides an effective means for the determination of electron-impact excitation cross sections. However, for complex atomic species, the number of levels that must be included in the configuration-interaction expansion of the N-electron target and the number of levels required in the close-coupling expansion for the $(N + 1)$-electron scattering system often renders these calculations extremely time consuming or even totally impractical. For this reason, methods such as those employed in the program JAJOM (Saraph 1972, 1978), that are based on the transformation of LS-coupling physical S- or K-matrices to intermediate coupling, have often been employed to generate approximate level-to-level cross sections. However, such transformation methods have significant problems that have severely limited their use (see Griffin *et al* 1998 for details).

Recently, we introduced what we refer to as the intermediate-coupling frame transformation (ICFT) method (Griffin *et al* 1998). It is based on the application of multi-channel quantum defect theory (MQDT) to first generate unphysical K-matrices in pure LS coupling. These unphysical K-matrices ($\mathcal{K}$) are then transformed to intermediate coupling and the physical K-matrices ($\boldsymbol{K}$) are finally determined from the equation:

$$\boldsymbol{K} = \mathcal{K}_{oo} - \mathcal{K}_{oc}[\mathcal{K}_{cc} + \tan(\pi\nu)]^{-1}\mathcal{K}_{co}, \tag{1}$$

where the matrices are partitioned by the open (o) and closed (c) channels; ν denotes the effective quantum numbers of the levels; and $\tan(\pi\nu)$ is a diagonal matrix. This method eliminates many of the problems associated with the transformation of physical S- or K-matrices and is capable of generating accurate level-to-level cross sections in much less time than that required for a full Breit–Pauli R-matrix calculation.

0953-4075/99/092139+14$19.50

In our earlier paper, we performed an 8-term, 14-level model calculation on Fe^{14+} in order to test the accuracy of the ICFT method in comparison to a Breit–Pauli calculation. We have now completed much more extensive ICFT calculations on the Mg-like ions Si^{2+}, Ar^{6+}, Ti^{10+} and Fe^{14+}, in which we have included 25-terms and 45-levels in both our configuration-interaction expansions and our close-coupling expansions. In the case of Fe^{14+}, we have also performed a Breit–Pauli calculation and we have compared the results from this calculation with those obtained from a far less time consuming ICFT calculation.

The remainder of this paper is organized as follows. In section 2, we discuss our atomic structure and scattering calculations for these four ions and present some of our results for energies, radiative rates and effective collision strengths for Si^{2+} and Fe^{14+}. In section 3, we consider line-emission intensity ratios as can be obtained using a collisional–radiative program such as that included in the Atomic Data and Analysis Structure (ADAS)—Summers (1994). Finally in section 4, we summarize our findings.

2. Atomic theory

2.1. Bound-state calculations

The bound-state radial wavefunctions for all four Mg-like ions included in this study were calculated using Froese Fischer's Hartree–Fock program (Froese Fischer 1991). The 1s, 2s, 2p and 3s orbitals were generated from a configuration-average Hartree–Fock (CAHF) calculation on the configuration $3s^2$; while the 3p, 3d, 4s, 4p and 4d orbitals were determined from CAHF frozen-core calculations on the configurations 3s3p, 3s3d, 3s4s, 3s4p and 3s4d, respectively. The bound-state energies and radiative rates were calculated from configuration-interaction Breit–Pauli calculations that included the 25 even-parity levels arising from the configurations $3s^2$, $3p^2$, 3s3d, 3s4s, 3s4d and $3d^2$; and the 20 odd-parity levels arising from the configurations 3s3p, 3p3d and 3s4p. In Si^{2+}, the nine levels of the $3d^2$ configuration are autoionizing, while in the other three ions they are bound.

In tables 1 and 2, we present our calculated energies for the bound levels of Si^{2+} and Fe^{14+}, respectively, in comparison with available experimental data (Martin and Zalubas 1983 for Si^{2+}, Sugar and Corliss 1985 for Fe^{14+}). As can be seen, our results for these two ions are in quite good agreement with the experimental energies. To obtain further improvement would require a much larger basis set, and this would significantly complicate our scattering calculations. The agreement between experiment and theory for the energies of the levels of Ar^{6+} and Ti^{10+} are comparable with the results presented here for Si^{2+} and Fe^{14+}.

In table 3, we present our radiative rates calculated in the length gauge for a set of selected transitions in Si^{2+} in comparison with the calculated rates for these transitions presented by Dufton *et al* (1983). The data of Dufton *et al* (1983) were chosen for comparison because their collisional–radiative modelling calculations as well as those of Kenan *et al* (1989) for this ion were based on these particular radiative rates. With the exception of the intercombination line $3s3p\ ^3P_1 \rightarrow 3s^2\ ^1S_0$, the rates given in Dufton *et al* (1983) were taken from the calculations of Baluja and Hibbert (1980). The rate for the transition $3s3d\ ^1D_2 \rightarrow 3s3p\ ^1P_1$ was not given in Dufton *et al* (1983), but was determined from the calculated energies and the oscillator strength presented by Baluja and Hibbert (1980). We see that the rates for the $3s3p\ ^3P_1 \rightarrow 3s^2\ ^1S_0$ and $3s4s\ ^1S_0 \rightarrow 3s3p\ ^1P_1$ transitions differ substantially, but the average deviation between the rates for the other nine transitions is only 3.5%. We will consider this comparison again in section 3. We have also calculated the radiative rates for Si^{2+} in the velocity gauge and found that for the ten dipole-allowed transitions shown in table 3, they differ from these results in the length gauge by an average of 12%. On the basis of these comparisons and others that we have

Table 1. Energies in eV relative to the ground level of the 36 bound levels included in the 45-state R-matrix close-coupling calculation on Si^{2+}.

Index	Level	Theor. energy	Expt [a] energy	Index	Level	Theor. energy	Expt [a] energy
1	$3s2\ ^1S_0$	0.00	0.00	2	$3s3p\ ^3P_0$	6.31	6.54
3	$3s3p\ ^3P_1$	6.32	6.55	4	$3s3p\ ^3P_2$	6.35	6.59
5	$3s3p\ ^1P_1$	10.56	10.28	6	$3p^2\ ^1D_2$	14.87	15.15
7	$3p^2\ ^3P_0$	15.88	16.08	8	$3p^2\ ^3P_1$	15.93	16.10
9	$3p^2\ ^3P_2$	15.96	16.13	10	$3s3d\ ^3D_1$	17.74	17.72
11	$3s3d\ ^3D_2$	17.74	17.72	12	$3s3d\ ^3D_3$	17.74	17.72
13	$3s4s\ ^3S_1$	19.01	19.01	14	$3p^2\ ^1S_0$	19.36	19.02
15	$3s4s\ ^1S_0$	20.32	19.73	16	$3s3d\ ^1D_2$	21.27	20.55
17	$3s4p\ ^3P_0$	21.70	21.73	18	$3s4p\ ^3P_1$	21.70	21.73
19	$3s4p\ ^3P_2$	21.71	21.74	20	$3s4p\ ^1P_1$	22.23	21.88
21	$3p3d\ ^3F_2$	24.91	24.66	22	$3p3d\ ^3F_3$	24.92	24.68
23	$3s4d\ ^3D_1$	24.94	25.00	24	$3s4d\ ^3D_2$	24.94	25.00
25	$3s4d\ ^3D_3$	24.94	25.00	26	$3p3d\ ^3F_4$	24.94	24.69
27	$3p3d\ ^1D_2$	25.23	25.42	28	$3s4d\ ^1D_2$	25.65	25.00
29	$3p3d\ ^3P_2$	26.78	26.80	30	$3p3d\ ^3P_1$	26.80	26.82
31	$3p3d\ ^3P_0$	26.80	26.82	32	$3p3d\ ^3D_1$	26.92	26.95
33	$3p3d\ ^3D_2$	26.93	26.96	34	$3p3d\ ^3D_3$	26.93	26.97
35	$3p3d\ ^1F_3$	29.58	—	36	$3p3d\ ^1P_1$	30.25	—

[a] Martin and Zalubas (1983).

made for the radiative rates in Si^{2+}, we estimate that our radiative rates for the dipole-allowed transitions between the lowest 16 levels shown in table 1 should be accurate to better than 20%. However, the radiative rates for dipole-allowed transitions involving the upper 20 levels in table 1 will be somewhat more uncertain because of the lack of configuration mixing with still higher levels. The dipole-forbidden transitions should only be considered estimates since they depend critically on very weak spin–orbit mixing of the levels.

In table 4, we show our radiative rates calculated in the length gauge for transitions to $3s^2\ ^1S_0$, $3s3p\ ^3P_{0,1,2}$ and $3s3p\ ^1P_1$ in Fe^{14+}. We have compared our results with the rates included in the NIST data base (Fuhr *et al* 1988), since they are widely available on the Internet, as well as to a set of rates determined from some of the oscillator strengths calculated by Deb and Msezane (1998). The agreement between our rates and those in the NIST data base is, in general, quite good; however, the accuracy ratings associated with the NIST data for this ion are not very high, especially for weak transitions that are only possible due to spin–orbit mixing of the levels. The oscillator strengths for the transitions by Deb and Msezane (1998) were determined using a 45-term, 87-level calculation and therefore those rates should be expected to be more accurate than our results determined from a 25-term, 45-level calculation. Our radiative rates differ from those of Deb and Msezane by 10% on average. We have also calculated these rates in the velocity gauge and found that, for the dipole-allowed transitions shown in table 4, they differ from the rates calculated in the length gauge by an average of 7%. On the basis of these comparisons, we estimate that the radiative rates for all dipole-allowed transitions between the levels given in table 2, should be accurate to about 15%. This improved accuracy is primarily due to the reduced effects of correlation in this highly ionized species. The spin–orbit mixing is much stronger in this fifteen times ionized species and the accuracy of the spin-forbidden transitions should be better than in the case of Si^{2+}. Indeed, we have found that the agreement between the rates determined in the length and velocity gauges for the

Table 2. Energies in eV relative to the ground level of all levels included in the 45-state R-matrix close-coupling calculation on Fe^{14+}.

Index	Level	Theor. Energy	Expt [a] Energy	Index	Level	Theor. Energy	Expt [a] Energy
1	$3s2\ ^1S_0$	0.00	0.00	2	$3s3p\ ^3P_0$	28.79	29.00
3	$3s3p\ ^3P_1$	29.48	29.71	4	$3s3p\ ^3P_2$	31.14	31.47
5	$3s3p\ ^1P_1$	44.06	43.63	6	$3p^2\ ^3P_0$	68.77	68.74
7	$3p^2\ ^1D_2$	69.19	69.38	8	$3p^2\ ^3P_1$	69.91	70.00
9	$3p^2\ ^3P_2$	71.87	72.12	10	$3p^2\ ^1S_0$	82.19	81.78
11	$3s3d\ ^3D_1$	84.60	84.16	12	$3s3d\ ^3D_2$	84.75	84.28
13	$3s3d\ ^3D_3$	84.99	84.48	14	$3s3d\ ^1D_2$	96.02	94.49
15	$3p3d\ ^3F_2$	115.28	115.11	16	$3p3d\ ^3F_3$	116.46	116.32
17	$3p3d\ ^1D_2$	117.73	—	18	$3p3d\ ^3F_4$	117.81	117.74
19	$3p3d\ ^3D_1$	122.39	—	20	$3p3d\ ^3P_2$	122.47	—
21	$3p3d\ ^3D_3$	123.84	—	22	$3p3d\ ^3P_0$	123.87	—
23	$3p3d\ ^3P_1$	123.93	—	24	$3p3d\ ^3D_2$	124.01	—
25	$3p3d\ ^1F_3$	133.63	—	26	$3p3d\ ^1P_1$	135.17	—
27	$3d^2\ ^3F_2$	170.55	—	28	$3d^2\ ^3F_3$	170.79	—
29	$3d^2\ ^3F_4$	171.09	—	30	$3d^2\ ^1D_2$	175.05	—
31	$3d^2\ ^3P_0$	175.08	—	32	$3d^2\ ^3P_2$	175.18	—
33	$3d^2\ ^3P_1$	175.52	—	34	$3d^2\ ^1G_4$	176.12	—
35	$3d^2\ ^1S_0$	186.42	—	36	$3s4s\ ^3S_1$	219.42	218.67
37	$3s4s\ ^1S_0$	223.26	–	38	$3s4p\ ^3P_0$	234.11	—
39	$3s4p\ ^3P_1$	234.30	—	40	$3s4p\ ^3P_2$	234.97	—
41	$3s4p\ ^1P_1$	236.23	234.32	42	$3s4d\ ^3D_1$	253.07	251.85
43	$3s4d\ ^3D_2$	253.12	251.94	44	$3s4d\ ^3D_3$	253.23	252.08
45	$3s4d\ ^1D_2$	253.91	252.34				

[a] Sugar and Corliss (1985).

Table 3. Radiative rates for selected transitions in Si^{2+} in units of s^{-1}.

Transition	Present results	Dufton *et al* (1983)
$3s3p\ ^3P_1–3s^2\ ^1S_0$	0.92×10^4	1.46×10^4
$3s3p\ ^1P_1–3s^2\ ^1S_0$	2.77×10^9	2.67×10^9
$3p^2\ ^3P_1–3s3p\ ^3P_0$	7.89×10^8	7.64×10^8
$3p^2\ ^3P_0–3s3p\ ^3P_1$	2.31×10^9	2.27×10^9
$3p^2\ ^3P_1–3s3p\ ^3P_1$	5.89×10^8	5.71×10^8
$3p^2\ ^3P_2–3s3p\ ^3P_1$	5.94×10^8	5.74×10^8
$3p^2\ ^3P_1–3s3p\ ^3P_2$	9.72×10^8	9.45×10^8
$3p^2\ ^3P_2–3s3p\ ^3P_2$	1.77×10^9	1.71×10^9
$3p^2\ ^1D_2–3s3p\ ^1P_1$	2.31×10^7	2.43×10^7
$3s4s\ ^1S_0–3s3p\ ^1P_1$	1.81×10^8	2.84×10^8
$3s3d\ ^1D_2–3s3p\ ^1P_1$	5.06×10^9	(4.82×10^9)[a]

[a] Calculated from the energies and oscillator strength given in Baluja and Hibbert (1980).

dipole-forbidden transitions in this ion are much better than in the case of Si^{2+}, although not nearly as good as for the dipole-allowed transitions. Thus, when possible, plasma diagnostics using these data should still be based primarily on dipole-allowed radiative transitions.

For sake of brevity, we have not included here our calculated radiative rates for Ar^{6+} or Ti^{10+}. We estimate that the rates for all dipole-allowed transitions for these two ions should be good to about 20%, while the dipole-forbidden transitions are less accurate. All the energy

Table 4. Radiative rates for transitions to $3s^2\ ^1S_0$, $3s3p\ ^3P_{0,1,2}$, and $3s3p\ ^1P_1$ for Fe^{14+} in units of s^{-1}.

Upper level	Lower level	Present results	NIST[a]	DM[b]
$3s3p\ ^3P_1$	$3s^2\ ^1S_0$	3.55×10^7	4.1×10^7	—
$3s3p\ ^1P_1$	$3s^2\ ^1S_0$	2.28×10^{10}	2.28×10^{10}	2.22×10^{10}
$3s4p\ ^1P_1$	$3s^2\ ^1S_0$	2.79×10^{11}	2.94×10^{11}	2.29×10^{11}
$3p^2\ ^3P_1$	$3s3p\ ^3P_0$	7.10×10^9	6.9×10^9	6.29×10^9
$3s3d\ ^3D_1$	$3s3p\ ^3P_0$	1.42×10^{10}	1.38×10^{10}	1.36×10^{10}
$3s4s\ ^3S_1$	$3s3p\ ^3P_0$	2.80×10^{10}	3.20×10^{10}	—
$3s4d\ ^3D_1$	$3s3p\ ^3P_0$	1.92×10^{11}	—	2.33×10^{11}
$3p^2\ ^1D_2$	$3s3p\ ^3P_1$	1.10×10^9	1.1×10^9	—
$3p^2\ ^3P_0$	$3s3p\ ^3P_1$	1.85×10^{10}	1.77×10^{10}	—
$3p^2\ ^3P_1$	$3s3p\ ^3P_1$	5.03×10^9	4.91×10^9	—
$3p^2\ ^3P_2$	$3s3p\ ^3P_1$	4.54×10^9	4.5×10^9	4.85×10^9
$3p^2\ ^1S_0$	$3s3p\ ^3P_1$	2.82×10^8	3.2×10^8	—
$3s3d\ ^3D_1$	$3s3p\ ^3P_1$	1.02×10^{10}	9.8×10^9	—
$3s3d\ ^3D_2$	$3s3p\ ^3P_1$	1.85×10^{10}	1.80×10^{10}	1.77×10^{10}
$3s3d\ ^1D_2$	$3s3p\ ^3P_1$	3.04×10^8	3.5×10^8	—
$3s4s\ ^3S_1$	$3s3p\ ^3P_1$	8.50×10^{10}	9.80×10^{10}	—
$3s4d\ ^3D_2$	$3s3p\ ^3P_1$	2.61×10^{11}	—	3.11×10^{11}
$3p^2\ ^1D_2$	$3s3p\ ^3P_2$	2.03×10^9	2.0×10^9	—
$3p^2\ ^3P_1$	$3s3p\ ^3P_2$	7.40×10^9	7.1×10^9	—
$3p^2\ ^3P_2$	$3s3p\ ^3P_2$	1.30×10^{10}	1.30×10^{10}	1.34×10^{10}
$3s3d\ ^3D_1$	$3s3p\ ^3P_2$	6.25×10^8	6.2×10^8	—
$3s3d\ ^3D_2$	$3s3p\ ^3P_2$	5.70×10^9	5.5×10^9	—
$3s3d\ ^3D_3$	$3s3p\ ^3P_2$	2.30×10^{10}	2.20×10^{10}	2.18×10^{10}
$3s3d\ ^1D_2$	$3s3p\ ^3P_2$	1.15×10^7	1.6×10^7	—
$3s4s\ ^3S_1$	$3s3p\ ^3P_2$	1.48×10^{11}	1.60×10^{11}	—
$3s4d\ ^3D_3$	$3s3p\ ^3P_2$	3.56×10^{11}	—	4.11×10^{11}
$3p^2\ ^1D_2$	$3s3p\ ^1P_1$	1.50×10^9	1.6×10^9	—
$3p^2\ ^3P_0$	$3s3p\ ^1P_1$	5.37×10^7	6.4×10^7	—
$3p^2\ ^3P_1$	$3s3p\ ^1P_1$	7.23×10^6	8.4×10^6	—
$3p^2\ ^3P_2$	$3s3p\ ^1P_1$	4.51×10^8	4.7×10^8	—
$3p^2\ ^1S_0$	$3s3p\ ^1P_1$	2.00×10^{10}	1.97×10^{10}	2.10×10^{10}
$3s3d\ ^3D_1$	$3s3p\ ^1P_1$	2.26×10^7	2.6×10^7	—
$3s3d\ ^3D_2$	$3s3p\ ^1P_1$	1.68×10^7	3.0×10^7	—
$3s3d\ ^1D_2$	$3s3p\ ^1P_1$	4.41×10^{10}	4.20×10^{10}	4.36×10^{10}
$3s4s\ ^1S_0$	$3s3p\ ^1P_1$	2.57×10^{11}	1.90×10^{11}	—
$3s4d\ ^1D_2$	$3s3p\ ^1P_1$	3.12×10^{11}	3.40×10^{11}	2.49×10^{11}

[a] Fuhr *et al* (1988).
[b] Deb and Msezane (1998).

levels and radiative rates for all four ions are now available on the Internet in ADAS format at the Oak Ridge National Laboratory (ORNL) Controlled Fusion Atomic Data Centre (CFADC)†.

2.2. Excitation calculations

The effective collision strength, Υ, first introduced by Seaton (1953) is defined by the equation

$$\Upsilon_{ij} = \int_0^\infty \Omega(i \rightarrow j) \exp\left(\frac{-\epsilon_j}{kT_e}\right) \mathrm{d}\left(\frac{\epsilon_j}{kT_e}\right), \tag{2}$$

† Webpage html: www-cfadc.phy.ornl.gov/data_and_codes

where Ω is the collision strength for the transition from level i to level j and ϵ_j is the continuum energy of the final scattered electron. It is this effective collision strength that is used for the input of excitation data to the ADAS suite of programs (Summers 1994) that we employ to carry out collisional–radiative modelling. It is especially convenient for interpolation with respect to the electron temperature, T_e, because it has a much more gradual variation with temperature than that of the rate coefficient.

The rate coefficients for collisional excitation $q_{i\to j}$ and de-excitation $q_{j\to i}$ can then be determined from the equations

$$q_{i\to j} = \frac{2\sqrt{\pi}\alpha c a_0^2}{\omega_i}\sqrt{\frac{I_H}{kT_e}}\exp\left(-\frac{\Delta E_{ij}}{kT_e}\right)\Upsilon_{ij}, \tag{3}$$

and

$$q_{j\to i} = \frac{\omega_i}{\omega_j}\exp\left(\frac{\Delta E_{ij}}{kT_e}\right)q_{i\to j}, \tag{4}$$

where $2\sqrt{\pi}\alpha c a_0^2 = 2.1716\times10^{-8}$ cm^3 s^{-1}, $I_H = 13.6058$ eV, ΔE_{ij} is the threshold energy for the transition from level i to level j, and ω_i and ω_j are the statistical weights of level i and level j, respectively. These rate coefficients are calculated internally in ADAS from the values of the effective collision strengths.

We now describe the computational procedures we used to determine the effective collision strengths. For all four Mg-like ions, we performed excitation calculations using the intermediate-coupling frame transformation (ICFT) method, which has been summarized in section 1 and described in detail in Griffin *et al* (1998). In order to further test the accuracy of this method, we also performed a full Breit–Pauli calculation for Fe^{14+}. For the LS portion of the ICFT calculations, we performed full-exchange calculations on all $LS\Pi$ partial waves up to $L = 12$. This allowed us to generate the contributions from all $J\Pi$ partial waves from $J = 0.5$–10.5 through our transformation technique. The LS close-coupling expansions included all 25 terms arising from the configurations $3s^2$, 3s3p, $3p^2$, 3s3d, 3p3d, $3d^2$, 3s4s, 3s4p and 3s4d. In the case of Fe^{14+}, we performed our Breit–Pauli calculation with full exchange for all $J\Pi$ partial waves from $J = 0.5$–10.5 and the close-coupling expansion included all 45 levels listed in table 2.

For all four ions, we employed 25 basis orbitals to represent the continuum for each value of the total orbital angular momentum, and the radius of the R-matrix box was equal to 22.05 au for Si^{2+}, 9.47 au for Ar^{6+}, 6.07 au for Ti^{10+} and 4.49 au for Fe^{14+}. It is also important to note that we do include the long-range potentials perturbatively within the context of MQDT in our modified version of the unpublished asymptotic code STGF (Seaton 1985), using methods described in the appendix of Gorczyca *et al* (1996). For these ions, the long-range potentials have been found to make important contributions to the collision strengths.

The expansion in $J\Pi$ partial waves up to $J = 10.5$ is not sufficiently complete for the determination of effective collision strengths, especially for transitions between excited levels where the threshold energies are relatively low. For this reason, we have also performed no-exchange calculations in LS coupling for $L = 10$–50, and used the unphysical K-matrices from this calculation and the ICFT method to determine the contributions for $J = 11.5$–48.5. These high J contributions were then topped-up as follows: the dipole transitions were topped-up using a method originally described by Burgess (1974) for LS coupling, but which we have implemented in intermediate coupling as well, while the non-dipole transitions were topped-up assuming a geometric series in J. Finally, these high partial-wave results were added to the results from our calculations for the low $J\Pi$ partial waves to determine the final collision strengths.

One of the difficulties associated with these calculations is obtaining a sufficiently fine energy mesh to resolve the resonance structures. This problem is more severe for highly ionized species where the width of the resonances can become especially narrow. If the mesh is too coarse, one can miss some resonance contributions and this will cause the calculated effective collision strengths to be too small. Conversely, one can also pick up a resonance that is actually narrower than the separation between adjacent mesh points, causing the resonance contribution to the calculated effective collision strength to be overestimated. These problems arising from an insufficiently fine energy mesh in the resonance region are of course most pronounced for weaker non-dipole transitions, where the contribution from direct excitation is relatively small.

We tested for problems associated with the energy mesh in the following way. We first calculated the effective collision strengths from equation (2), using a file of collision strengths calculated using a given energy mesh; we then eliminated any resonances from this file that had widths less than or equal to the separation between adjacent mesh points. If the effective collisions strengths from these two calculations changed significantly, we employed a finer energy mesh.

We were able to use sufficiently fine meshes in the case of Si^{2+}, Ar^{6+} and Ti^{10} so that the differences between the two sets of effective collision strengths were small. In fact, the results were nearly identical for all transitions in the case of Si^{2+}; for Ar^{6+} and Ti^{10+}, they differed by around 10% for a few of the weaker transitions at the lowest temperatures, but were much closer for the vast majority of transitions. However, as expected, more mesh points were required within the resonance region in the case of Ti^{10+} than for Si^{2+} or Ar^{6+}.

For Fe^{14+} the problems associated with the energy mesh were somewhat more pronounced. Even with the inclusion of 10 000 mesh points within the resonance region, we found that the effective collision strengths for a few of the weakest transitions, calculated in the two ways described above, differed by between 30 and 40% at the lower temperatures. However, the vast majority of the effective collision strengths were very close and it was decided not to go to a finer mesh because of the amount of computational time involved, especially for the Breit–Pauli calculation.

Next we consider the results of our excitation calculations for Fe^{14+}. It is important to note that with the number of levels included in this calculation, the Breit–Pauli calculation was extremely time consuming, mainly due to the size of the $(N + 1)$-electron matrix that must be diagonalized inside the R-matrix box for each value of J and Π. The inner-region portion of the Breit–Pauli calculation took about 38 times as long as the same portion of the ICFT calculation in LS coupling, while the asymptotic part of the Breit–Pauli calculation for 10 000 energy mesh points took about 2.5 times as long as the asymptotic part of the ICFT calculation. With fewer mesh points, the savings associated with the ICFT method for the asymptotic part of the problem was even more significant. In addition, it is worth noting that the asymptotic portion of our Breit–Pauli calculation was also performed using MQDT (see Badnell *et al* 1998), and this affords significant time savings over the standard asymptotic methods employed in R-matrix calculations. Thus the savings in computational time for the ICFT method over standard Breit–Pauli R-matrix calculations would be even more significant.

In table 5, we compare Breit–Pauli and ICFT effective collision strengths from the $3s^2\ ^1S_0$ ground level to the levels of the configurations 3s3p, $3p^2$, 3s3d and 3s4s in Fe^{14+}. Overall, the agreement between these two sets of effective collision strengths is very good. The largest differences occur for the weak excitation to the $3p^2\ ^3P_0$ level at lower temperatures. These are due primarily to differences in the very narrow resonance structures between these two calculations. The average difference of the ICFT results from the Breit–Pauli results for the data shown in this table is 2.4%. This is probably smaller than the uncertainty associated with

Table 5. Effective collision strengths from level $3s^2\ ^1S_0$ to the levels of the configurations 3s3p, $3p^2$, 3s3d and 3s4s in Fe^{14+} from a Breit–Pauli calculation (first row) and from an ICFT calculation (second row).

	Electron temperature (K)						
To level	2.25×10^5	4.50×10^5	1.13×10^6	2.25×10^6	4.50×10^6	1.13×10^7	2.25×10^7
$3s3p\ ^3P_0$	1.96×10^{-2}	1.45×10^{-2}	9.07×10^{-3}	6.01×10^{-3}	3.83×10^{-3}	2.00×10^{-3}	1.18×10^{-3}
	2.00×10^{-2}	1.52×10^{-2}	9.49×10^{-3}	6.26×10^{-3}	3.96×10^{-3}	2.05×10^{-3}	1.21×10^{-3}
$3s3p\ ^3P_1$	1.28×10^{-1}	9.20×10^{-2}	5.83×10^{-2}	4.21×10^{-2}	3.19×10^{-2}	2.40×10^{-2}	2.05×10^{-2}
	1.26×10^{-1}	9.24×10^{-2}	5.93×10^{-2}	4.30×10^{-2}	3.27×10^{-2}	2.47×10^{-2}	2.14×10^{-2}
$3s3p\ ^3P_2$	1.12×10^{-1}	8.88×10^{-2}	5.56×10^{-2}	3.61×10^{-2}	2.24×10^{-2}	1.13×10^{-2}	6.57×10^{-3}
	1.02×10^{-1}	8.22×10^{-2}	5.22×10^{-2}	3.41×10^{-2}	2.13×10^{-2}	1.09×10^{-2}	6.35×10^{-3}
$3s3p\ ^1P_1$	2.76×10^{0}	2.81×10^{0}	2.85×10^{0}	2.92×10^{0}	3.01×10^{0}	3.08×10^{0}	3.08×10^{0}
	2.78×10^{0}	2.82×10^{0}	2.86×10^{0}	2.92×10^{0}	3.01×10^{0}	3.08×10^{0}	3.11×10^{0}
$3p^2\ ^3P_0$	1.09×10^{-3}	7.58×10^{-4}	4.37×10^{-4}	3.48×10^{-4}	4.70×10^{-4}	6.75×10^{-4}	6.62×10^{-4}
	1.44×10^{-3}	9.68×10^{-4}	5.26×10^{-4}	3.90×10^{-4}	4.89×10^{-4}	6.84×10^{-4}	6.70×10^{-4}
$3p^2\ ^1D_2$	1.03×10^{-1}	9.67×10^{-2}	8.97×10^{-2}	8.73×10^{-2}	8.59×10^{-2}	7.56×10^{-2}	6.04×10^{-2}
	1.03×10^{-1}	9.68×10^{-2}	8.96×10^{-2}	8.73×10^{-2}	8.59×10^{-2}	7.59×10^{-2}	6.09×10^{-2}
$3p^2\ ^3P_1$	2.01×10^{-3}	1.39×10^{-3}	7.09×10^{-4}	3.97×10^{-4}	2.16×10^{-4}	9.54×10^{-5}	5.10×10^{-5}
	2.01×10^{-3}	1.38×10^{-3}	7.00×10^{-4}	3.91×10^{-4}	2.13×10^{-4}	9.39×10^{-5}	5.03×10^{-5}
$3p^2\ ^3P_2$	2.38×10^{-2}	2.18×10^{-2}	1.97×10^{-2}	1.89×10^{-2}	1.85×10^{-2}	1.62×10^{-2}	1.30×10^{-2}
	2.37×10^{-2}	2.17×10^{-2}	1.96×10^{-2}	1.89×10^{-2}	1.85×10^{-2}	1.63×10^{-2}	1.31×10^{-2}
$3p^2\ ^1S_0$	1.02×10^{-2}	7.93×10^{-3}	5.46×10^{-3}	4.08×10^{-3}	3.10×10^{-3}	2.11×10^{-3}	1.50×10^{-3}
	1.02×10^{-2}	8.03×10^{-3}	5.49×10^{-3}	4.08×10^{-3}	3.09×10^{-3}	2.11×10^{-3}	1.50×10^{-3}
$3s3d\ ^3D_1$	1.44×10^{-2}	1.38×10^{-2}	1.13×10^{-2}	8.60×10^{-3}	6.06×10^{-3}	3.47×10^{-3}	2.16×10^{-3}
	1.43×10^{-2}	1.39×10^{-2}	1.14×10^{-2}	8.64×10^{-3}	6.08×10^{-3}	3.49×10^{-3}	2.17×10^{-3}
$3s3d\ ^3D_2$	2.37×10^{-2}	2.30×10^{-2}	1.89×10^{-2}	1.44×10^{-2}	1.02×10^{-2}	5.83×10^{-3}	3.63×10^{-3}
	2.42×10^{-2}	2.34×10^{-2}	1.92×10^{-2}	1.46×10^{-2}	1.02×10^{-2}	5.87×10^{-3}	3.65×10^{-3}
$3s3d\ ^3D_3$	3.26×10^{-2}	3.16×10^{-2}	2.61×10^{-2}	2.00×10^{-2}	1.41×10^{-2}	8.09×10^{-3}	5.03×10^{-3}
	3.31×10^{-2}	3.21×10^{-2}	2.64×10^{-2}	2.01×10^{-2}	1.42×10^{-2}	8.13×10^{-3}	5.06×10^{-3}
$3s3d\ ^1D_2$	1.97×10^{-1}	1.98×10^{-1}	1.94×10^{-1}	1.95×10^{-1}	1.96×10^{-1}	1.75×10^{-1}	1.41×10^{-1}
	1.94×10^{-1}	1.95×10^{-1}	1.92×10^{-1}	1.94×10^{-1}	1.96×10^{-1}	1.76×10^{-1}	1.42×10^{-1}
$3s4s\ ^3S_1$	1.07×10^{-2}	6.88×10^{-3}	3.87×10^{-3}	2.59×10^{-3}	1.73×10^{-3}	9.73×10^{-4}	6.10×10^{-4}
	9.93×10^{-3}	6.48×10^{-3}	3.70×10^{-3}	2.50×10^{-3}	1.68×10^{-3}	9.57×10^{-4}	6.04×10^{-4}
$3s4s\ ^1S_0$	7.91×10^{-2}	7.18×10^{-2}	7.61×10^{-2}	8.28×10^{-2}	8.55×10^{-2}	7.59×10^{-2}	6.06×10^{-2}
	7.92×10^{-2}	7.18×10^{-2}	7.62×10^{-2}	8.28×10^{-2}	8.55×10^{-2}	7.62×10^{-2}	6.11×10^{-2}

unresolved resonances discussed above. Since there are no experimental data with which to compare our calculated excitation cross sections or other theoretical effective collision strengths for this ion, it is somewhat difficult to estimate the overall accuracy of our results. However, we would estimate that the effective collision strengths for the dipole-allowed excitations should be accurate to at least 20%. As we will discuss in section 3, the accuracy of these data for the non-dipole allowed transitions are somewhat less certain because of uncertainties associated with the very strong resonant contributions to these transitions.

We now consider briefly our ICFT calculations for Si^{2+}, Ar^{6+} and Ti^{10+}. It should be noted here that in our earlier work on the low-energy differential and total excitation cross sections in *LS* coupling for Si^{2+} and Ar^{6+}, we employed quite different basis sets (see Griffin *et al* 1993). However, the total cross sections for excitation to the ^3P and ^1P terms presented in that study are in good agreement with the present results, although the details of some of the resonance structures are slightly different. Furthermore, those results agree well with the low-energy

Table 6. Effective collision strengths from level $3s^2\ ^1S_0$ to the levels of 3s3p, $3p^2$, 3s3d and 3s4s in Si^{2+} from an ICFT calculation.

	Electron temperature (K)						
To level	9.00×10^3	1.80×10^4	4.50×10^4	9.00×10^4	1.80×10^5	4.50×10^5	9.00×10^5
$3s3p\ ^3P_0$	7.37×10^{-1}	5.90×10^{-1}	4.12×10^{-1}	2.90×10^{-1}	1.90×10^{-1}	9.97×10^{-2}	5.86×10^{-2}
$3s3p\ ^3P_1$	2.25×10^{0}	1.78×10^{0}	1.24×10^{0}	8.74×10^{-1}	5.72×10^{-1}	3.00×10^{-1}	1.75×10^{-1}
$3s3p\ ^3P_2$	3.83×10^{0}	3.00×10^{0}	2.07×10^{0}	1.46×10^{0}	9.54×10^{-1}	5.01×10^{-1}	2.94×10^{-1}
$3s3p\ ^1P_1$	5.77×10^{0}	6.43×10^{0}	7.48×10^{0}	8.53×10^{0}	1.02×10^{1}	1.42×10^{1}	1.78×10^{1}
$3p^2\ ^1D_2$	8.27×10^{-1}	8.81×10^{-1}	9.74×10^{-1}	1.04×10^{0}	1.13×10^{0}	1.30×10^{0}	1.30×10^{0}
$3p^2\ ^3P_0$	2.68×10^{-2}	2.31×10^{-2}	1.54×10^{-2}	9.94×10^{-3}	5.95×10^{-3}	2.80×10^{-3}	1.54×10^{-3}
$3p^2\ ^3P_1$	8.08×10^{-2}	6.99×10^{-2}	4.66×10^{-2}	3.00×10^{-2}	1.79×10^{-2}	8.40×10^{-3}	4.57×10^{-3}
$3p^2\ ^3P_2$	1.36×10^{-1}	1.17×10^{-1}	7.76×10^{-2}	5.00×10^{-2}	2.99×10^{-2}	1.42×10^{-2}	7.83×10^{-3}
$3s3d\ ^3D_1$	2.18×10^{-1}	2.03×10^{-1}	1.72×10^{-1}	1.43×10^{-1}	1.11×10^{-1}	7.14×10^{-2}	4.71×10^{-2}
$3s3d\ ^3D_2$	3.67×10^{-1}	3.41×10^{-1}	2.89×10^{-1}	2.40×10^{-1}	1.86×10^{-1}	1.19×10^{-1}	7.87×10^{-2}
$3s3d\ ^3D_3$	5.12×10^{-1}	4.78×10^{-1}	4.06×10^{-1}	3.36×10^{-1}	2.61×10^{-1}	1.67×10^{-1}	1.10×10^{-1}
$3s4s\ ^3S_1$	1.94×10^{-2}	1.37×10^{-2}	8.06×10^{-3}	5.32×10^{-3}	3.47×10^{-3}	1.89×10^{-3}	1.16×10^{-3}
$3p^2\ ^1S_0$	2.11×10^{-1}	1.94×10^{-1}	1.81×10^{-1}	1.79×10^{-1}	1.83×10^{-1}	1.92×10^{-1}	1.81×10^{-1}
$3s4s\ ^1S_0$	1.31×10^{-2}	1.27×10^{-2}	1.28×10^{-2}	1.32×10^{-2}	1.36×10^{-2}	1.30×10^{-2}	1.10×10^{-2}
$3s3d\ ^1D_2$	9.10×10^{-1}	9.14×10^{-1}	9.39×10^{-1}	9.68×10^{-1}	1.02×10^{0}	1.08×10^{0}	1.03×10^{0}

experimental measurements for excitation to the 3s3p ^{3}P and 3s3p ^{1}P levels in Si^{2+} (Wallbank *et al* 1997, Reisenfeld 1997) and excitation to the 3s3p ^{3}P and 3s3p ^{1}P levels in Ar^{6+} (Chung *et al* 1997).

Our calculated effective collision strengths for Si^{2+} for transitions from the ground level to the levels of the 3s3p, $3p^2$, 3s3d and 3s4s configurations are presented in table 6. We expect that the agreement between the results of a full Breit–Pauli calculation and these ICFT results for all possible transitions between the bound-state levels should be even better than in the case of Fe^{14+}, since the effects of the spin–orbit interaction are much smaller for this doubly ionized species. Furthermore, the overall accuracy of the effective collision strengths for transitions between the lower 16 levels shown in table 1 for Si^{2+} should be comparable with the accuracy of our Fe^{14+} results. However, the effective collision strengths for transitions to the upper 20 bound levels in table 1 are less accurate because of the greater importance of correlation in the ion with still higher levels not included in our configuration-interaction expansion of the target. Our effective collision strengths for Ar^{6+} and Ti^{10+} are not presented here but the accuracy of our results for these ions for all transitions should be comparable with that of Fe^{14+}. Along with the energy levels and radiative rates, the collision strengths for all transitions between the bound levels included in our calculations for these four Mg-like ions are available in ADAS format on the Internet at the site given above.

3. Emission-line intensity ratios

The radiative and collisional atomic data for Si^{2+}, Ar^{6+}, Ti^{10+} and Fe^{14+} described in section 2 may be used to predict level populations and emission-line intensity ratios for a range of electron densities and temperatures appropriate to many laboratory and astrophysical plasmas. The atomic data sets available at the ORNL CFADC web site are in a general format (adf04) developed to interface with the ADAS collisional–radiative modelling codes (Summers 1994). Quantum numbers and energies for each atomic level are listed first, followed by radiative rates and effective collision strengths for all possible pairs of levels. The effective collision

strengths are listed at eight electron temperatures selected on the basis of the ionization stage of the atomic species. Although specific for ADAS, the general nature of the atomic data format should allow easy incorporation into most plasma modelling codes.

A number of line-ratio studies have been made on Si^{2+} in order to interpret solar observational data. Dufton *et al* (1983) employed calculations of radiative rates by Baluja and Hibbert (1980) and collisional rates by Baluja *et al* (1980, 1981) to determine the four emission-line intensity ratios:

$$R_1 = \frac{3p^2\,{}^3P_1 \rightarrow 3s3p\,{}^3P_0}{3s3p\,{}^3P_1 \rightarrow 3s^2\,{}^1S_0},$$

$$R_2 = \frac{3p^2\,{}^3P_0 \rightarrow 3s3p\,{}^3P_1}{3s4s\,{}^1S_0 \rightarrow 3s3p\,{}^1P_1},$$

$$R_3 = \frac{3p^2\,{}^3P_0 \rightarrow 3s3p\,{}^3P_1}{3p^2\,{}^3P_1 \rightarrow 3s3p\,{}^3P_0},$$

and

$$R_4 = \frac{3p^2\,{}^3P_0 \rightarrow 3s3p\,{}^3P_1}{3p^2\,{}^3P_1 \rightarrow 3s3p\,{}^3P_2}.$$

In a later analysis, Keenan *et al* (1989) studied the effects of non-Maxwellian rates on these same four line ratios. These particular ratios were chosen because they all provide density diagnostics for electron densities greater than 10^{10} cm^{-3}, with R_1 and R_2 being the most sensitive to changes in density.

However, for purely *ab initio* calculations, both R_1 and R_2 are difficult to determine accurately. The radiative rate involved in the denominator of R_1 depends on very weak mixing between the 3s3p $^3P_1$ and 3s3p $^1P_1$ levels through the spin–orbit parameter of the 3p electron. Baluja and Hibbert (1980) originally determined a radiative rate for this transition of 1.21×10^4 s^{-1}, compared with our value of 0.94×10^4 s^{-1}. Kwong *et al* (1983) obtained an experimental value for this rate of 1.67×10^4 s^{-1}. Then, by repeating the calculation of Baluja and Hibbert (1980) with the diagonal energies of the Hamiltonian matrix adjusted to reproduce the experimental energies, Dufton *et al* (1983) arrived at an improved value of 1.46×10^4 s^{-1}. Finally, Ojha *et al* (1988) re-evaluated this rate using improvements on the methods employed by Baluja and Hibbert (1980) to obtain a value equal to the experimental rate. However, without accurate experimental rates as a guide, the use of very weak intercombination lines for the interpretation of plasma conditions is suspect.

The radiative rate in the denominator of R_2 is also very sensitive to the details of the calculation. For example, Baluja and Hibbert (1980) found that the oscillator strength for the 3s4s $^1S \rightarrow$ 3s3p ^1P transition was reduced by a factor of 2.4 when they included a 5s pseudo state in their calculation. The length and velocity values of their oscillator strengths were actually in slightly better agreement without the inclusion of this pseudo state, but it brought them into better agreement with the model potential calculation of Victor *et al* (1976). With this lower value of the oscillator strength and experimental energies, one obtains the radiative rate for this transition employed by Dufton *et al* (1983) of 2.84×10^8 s^{-1}. Repeating this procedure for the oscillator strength determined by Victor *et al* (1976), one obtains a rate of 2.03×10^8 s^{-1}. In comparison, our completely *ab initio* value for this rate is 1.81×10^8 s^{-1}. Thus, we again have an uncertainty in this radiative rate which could have an important impact on this calculated line ratio. Indeed, we obtained nearly a 50% reduction in this line ratio if we used the rate employed by Dufton *et al* (1983), rather than our value.

Of course, when selecting line ratios for the interpretation of astrophysical and laboratory plasmas, one must also be concerned about the accuracy of the collisional rates. Those

transitions with very weak direct excitation cross sections are often dominated by resonant contributions. The strength of the resonant contributions can often be very sensitive to the exact energies of the various resonant states; this has already been demonstrated in, the case of the $3s^2\,{}^1S \rightarrow 3s3p\,{}^3P$ excitation in the Mg-like ions (see Griffin *et al* 1994, Badnell *et al* 1994). Furthermore, as discussed in the last section, it is often difficult to find an energy mesh that is sufficiently fine to resolve the myriad of narrow resonances that tend to dominate these cross sections. Therefore, in this case, there is more uncertainty associated with the accuracy of effective collision strengths for excitation from the $3s^2\,{}^1S_0$ ground level to the $3s3p\,{}^3P$ and $3p^2\,{}^3P$ levels than the much stronger dipole excitations from the ground level.

However, for diagnostic purposes, the emission-line intensities from levels that are directly excited by strong dipole excitations tend to show much less density dependence than those that are directly excited by weaker non-dipole excitations. Thus all four of the line ratios employed by Dufton *et al* (1983) as density diagnostics involve upper levels that are directly excited by non-dipole transitions from the ground level. Furthermore, R_1, R_3, and R_4 involve the $3p^2\,{}^3P_1$ level and this can be populated by the indirect mechanism of excitation to the $3s3p\,{}^3P_0$ and $3s3p\,{}^3P_2$ metastable levels followed by strong dipole excitations from the metastables. Therefore they all show the needed density dependence but are less certain in terms of the accuracy of the theoretical collision strengths that most directly affect the populations of the upper levels.

Another possible line ratio for the analysis of plasma conditions in these ions was suggested to us by Raymond (1998) and is given by

$$R_5 = \frac{3p^2\,{}^3P_1 \rightarrow 3s3p\,{}^3P_0}{3s3p\,{}^1P_1 \rightarrow 3s^2\,{}^1S_0}.$$

The collisional and radiative rates which directly affect the denominator and the radiative rate which directly affects the numerator in this line ratio should be quite accurate. However, since the excitation cross section from $3s^2\,{}^1S_0$ to $3p^2\,{}^3P_1$ is completely dominated by narrow resonances, the accuracy of this collision strength is more uncertain. The same holds true for excitation from the ground level to the $3s3p\,{}^3P_0$ and $3s3p\,{}^3P_2$ metastable levels, which as mentioned above, can indirectly populate the $3p^2\,{}^3P_1$ level.

For Si^{2+}, Ar^{6+} and Ti^{10+}, we have found that our energy mesh is sufficiently fine to resolve most of the narrow resonant structures. In the case of Fe^{14+}, this is less sure. However, as can be seen from table 5, the agreement between the ICFT and Breit–Pauli collision strengths for excitation directly to $3p^2\,{}^3P_1$ is very good. On the other hand, the agreement between the Breit–Pauli and ICFT calculations with regard to the indirect mechanism for populating this level is less certain because of the somewhat larger differences between the effective collision strengths for the transitions from the ground level to the two metastable levels of $3s3p\,{}^3P$.

In figure 1, we illustrate the application of these collisional–radiative data by presenting our results for the line ratio R_5 as a function of temperature for all four atomic ions. The higher curve for each ion is calculated at an electron density of 10^{14} cm^{-3}, while the lower curve is for an electron density of 10^8 cm^{-3}. For both Si^{2+} and Ar^{6+} this particular line ratio may serve as a temperature diagnostic, as well as a density diagnostic for densities above 10^{10} cm^{-3}. However, the variation of this line ratio with both temperature and density decreases as a function of ionization stage. For Fe^{14+}, it still may be useful as a temperature diagnostic but clearly could not be employed for the detection of variations in density.

As a check on the electron impact excitation calculations, we have also compared the line ratios R_3, R_4 and R_5 for Fe^{14+} calculated from the ICFT effective collision strengths to these line ratios calculated using the Breit–Pauli effective collision strengths. The radiative rates are of course the same in each calculation. Differences in the line ratios are due primarily to small changes in the detailed resonance structures between the two calculations. Resonances in the

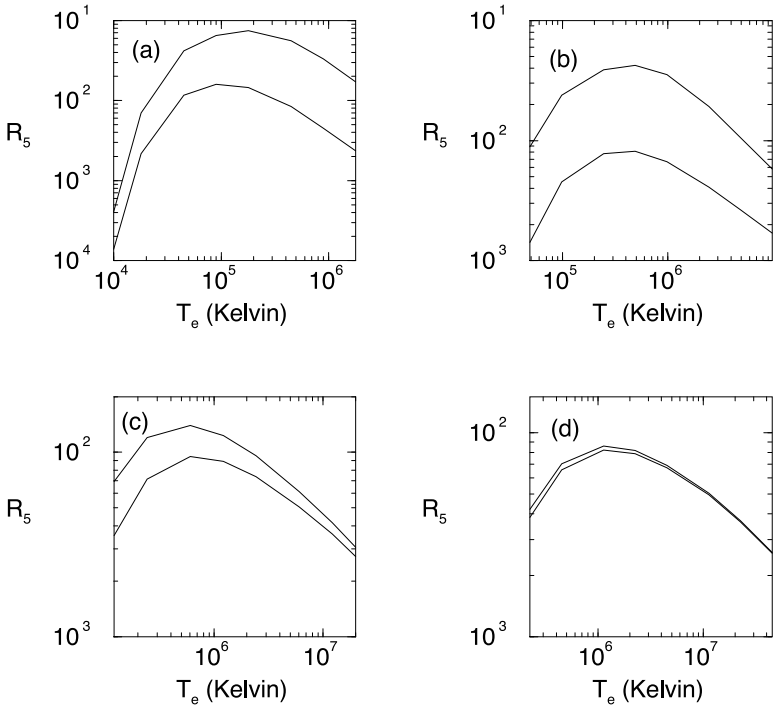

Figure 1. Line-emission intensity ratio R_5 for (*a*) Si^{2+}, (*b*) Ar^{6+}, (*c*) Ti^{10+} and (*d*) Fe^{14+}. For each ion, the lower curve corresponds to a density of 10^8 cm^{-3}, while the upper curve corresponds to a density of 10^{14} cm^{-3}.

cross sections affect the effective collision strengths for each ion studied here, but Fe^{14+} is the most sensitive to the details of the narrow resonances and the energy mesh size. The differences between the ICFT and Breit–Pauli calculations for the line ratios R_3 and R_4 were less than 15%, while these differences for R_5 are approximately 10%. In the case of R_3 and R_4, these are due both to variations in the collision strengths for the transition directly from the ground level to $3p^2\,{}^3P_0$ as well as the collision strengths from the ground level to the metastables, while in the case of R_5, they are caused almost entirely by variations in the collision strength to the metastables.

We have examined one other line ratio as a possible temperature diagnostic:

$$R_6 = \frac{3s3d\ {}^1D_2 \rightarrow 3s3p\ {}^1P_1}{3s3p\ {}^1P_1 \rightarrow 3s^2\ {}^1S_0}.$$

Although the effective collision strength to $3s3d\ {}^1D_2$ from the ground level is small compared with the effective collision strength to $3s3p\ {}^1P_1$ from the ground level, it is far less sensitive to the contributions from narrow resonances than, for example, the effective collision strength to the $3p^2\ {}^3P_0$ level. Furthermore, as can be seen from the comparisons given in tables 3 and 4, the radiative rate for the transition $3s3d\ {}^1D_2 \rightarrow 3s3p\ {}^1P_1$ appears to be fairly accurate. This line ratio is not useful in the case of Si^{2+} because the experimental wavelengths are within 0.01 Å of each other. However, for the other three ions considered here, these lines are well separated. Our calculations indicate that for densities below 10^{12} cm^{-3}, this line ratio is not sensitive to density; however, it could serve as a temperature diagnostic for Ar^{6+}, Ti^{10+} and Fe^{14+}.

4. Conclusions

We have completed extensive level-to-level Breit–Pauli calculations of radiative rates and ICFT calculations of effective collision strengths for the Mg-like ions Si^{2+}, Ar^{6+}, Ti^{10+} and Fe^{14+}. For Fe^{14+}, we have also determined the effective collision strengths using a full Breit–Pauli calculation and compared the results with the ICFT values. For almost all transitions, the ICFT and Breit–Pauli results are in excellent agreement. There are some differences in the effective collision strengths for a few of the weaker transitions and these are due to small differences in the detailed resonance structures.

We have also discussed the use of these data for line-ratio calculations and have presented our results for a selected line ratio. It is clear that line ratios for use in the interpretation of astrophysical and laboratory plasmas must be chosen not only on the basis of their wavelength range or their ability to reveal density or temperature dependence, but also on the basis of the accuracy of the underlying atomic data. This calls for close collaboration between those generating the data and those using it as a plasma diagnostic.

The ICFT method opens up the possibility of such studies for more complex atomic species that would be extremely time consuming or impractical using a full Breit–Pauli approach. However, further work is still needed to test the accuracy of this method with regard to the situation of low-lying resonances of one series embedded in high-lying resonances attached to a lower threshold when the energy dependence of the low-lying resonances is not factored-out by equation (1). Therefore, our next application of this method will focus on cases where there are large 'correlation' resonance structures in the low-energy regime.

Acknowledgments

In this work, DCG was supported by a US DoE Grant (DE-FG02-96-ER54367) with Rollins College and MSP and JAS were supported by a US DoE Grant (DE-FG05-96-ER54348) with Auburn University.

References

Badnell N R, Gorczyca T W and Price A D 1998 *J. Phys. B: At. Mol. Opt. Phys.* **31** L239–48
Badnell N R, Griffin D C, Gorczyca T W and Pindzola M S 1994 *Phys. Rev.* A **50** 1231–9
Baluja K L, Burke P G and Kingston A E 1980 *J. Phys. B: At. Mol. Opt. Phys.* **13** L543–5
——1981 *J. Phys. B: At. Mol. Opt. Phys.* **14** 1333–40
Baluja K L and Hibbert A 1980 *J. Phys. B: At. Mol. Opt. Phys.* **13** L327–9
Berrington K A, Eissner W B and Norrington P H 1995 *Comput. Phys. Commun.* **92** 290–420
Burgess A 1974 *J. Phys. B: At. Mol. Opt. Phys.* **7** L364–7
Chung Y-S, Djurić N, Wallbank B, Dunn G H, Bannister M E and Smith A C H 1997 *Phys. Rev.* A **55** 2044–9
Deb N C and Msezane A Z 1998 *J. Phys. B: At. Mol. Opt. Phys.* **31** L281–7
Dufton D L, Hibbert A, Kingston A E and Doschek G A 1983 *Astrophys. J.* **274** 420–8
Froese Fischer C 1991 *Comput. Phys. Commun.* **64** 369–519
Fuhr J R, Martin G A and Wiese W L 1988 *J. Phys. Chem. Ref. Data Suppl. 4* **17**
Gorczyca T W, Robicheaux F, Pindzola M S and Badnell N R 1996 *Phys. Rev.* A **54** 2107–15
Griffin D C, Badnell N R and Pindzola M S 1998 *J. Phys. B: At. Mol. Phys.* **31** 3713–27
Griffin D C, Pindzola M S and Badnell N R 1993 *Phys. Rev.* A **47** 2871–81
Griffin D C, Pindzola M S, Robicheaux F, Gorczyca T W and Badnell N R 1994 *Phys. Rev. Lett.* **72** 3491–4
Keenan F P, Cook J W, Dufton P L and Kingston A E 1989 *Astrophys. J.* **340** 1135–9
Kwong H W, Johnson B C, Smith P L and Parkinson W H 1983 *Phys. Rev.* A **27** 3040–3
Martin W C and Zalubas R 1983 *J. Phys. Chem. Ref. Data* **12** 323–80
Ojha P C, Keenan F P and Hibbert A 1988 *J. Phys. B: At. Mol. Opt. Phys.* **21** L395–401
Raymond J 1998 Private communication

Reisenfeld D 1997 Private communication
Saraph H E 1972 *Comput. Phys. Commun.* **3** 256–68
——1978 *Comput. Phys. Commun.* **15** 247–58
Seaton M J 1953 *Proc. R. Soc.* A **218** 400–16
——1985 *J. Phys. B: At. Mol. Opt. Phys.* **18** 2111–31
Sugar J and Corliss C 1985 *J. Phys. Chem. Ref. Data Suppl. 2* **14**
Summers H P 1994 *Atomic Data and Analysis Structure User Manual* JET-IR(94)06
Victor G A, Stewart R F and Laughlin C 1976 *Astrophys. J. Supl.* **31** 237–41
Wallbank B, Djuric N, Woitke O, Zhou S, Dunn G H, Smith A C H and Bannister M E 1997 *Phys. Rev.* A **56** 3714–18